



RESEARCH

Open Access



Spatial transcriptomics reveal high T cell and monocyte status as predictive and prognostic markers in pancreatic cancer

Yeon Bi Han^{1,2†}, Sejoon Lee^{1,3†}, Jin-Ok Lee⁴, Se In Jeong^{1,2}, Ki Rim Lee^{1,2,5}, Soomin Ahn⁶, Kwangrok Jung^{7,8}, Jong-Chan Lee^{7,8}, Yoo-Seok Yoon⁹, Jin-Hyeok Hwang^{7,8}, Ho-Seong Han⁹, Hee Young Na^{1,2*}  and Jaihwon Kim^{7,8*} 

Abstract

Background In the present study, we intended to discover predictive or prognostic factors of pancreatic ductal adenocarcinoma (PDAC). We intended to investigate the differences between PDAC cases that are treated with upfront surgery (UFS) and surgery after neoadjuvant FOLFIRINOX chemotherapy (NAT), and cases with good and poor responses to NAT, using digital spatial profiling (DSP) and immunohistochemical (IHC) analysis.

Methods Forty-eight PDAC cases that were surgically resected with or without NAT were included. A tissue microarray was constructed for DSP and IHC. Pathological tumor regression to NAT was graded based on the College of American Pathologists (CAP) system.

Results Between the UFS and NAT groups, there were no significant differentially expressed genes in all cell types. In the NAT group, *MFAP4* and *EGR3* were upregulated in CAP 2 in pan CK- and CD45-negative cells. Gene set enrichment analysis of CD45-positive cells showed that genes related to B or T cell-associated pathways were enriched in CAP 2, which correlated with the IHC; higher CD3-, CD4-, and CD8-positive cell densities in CAP 2. Multivariate analysis revealed age, high monocyte infiltration, and high CD68-positive cell infiltration as independent prognostic factors for overall survival.

Conclusions Increased expression of *MFAP4* and *EGR3* as well as high CD3-, CD4-, and CD8-positive cell infiltration may be predictive markers of the NAT response in PDAC. Additionally, high monocyte infiltration and high CD68-positive cell infiltration could serve as prognostic markers for PDAC.

Keywords Pancreatic cancer, Spatial transcriptomics, Immunohistochemistry, Predictive marker, Prognostic marker

[†]Yeon Bi Han and Sejoon Lee contributed equally to this work as the first authors. Hee Young Na and Jaihwon Kim contributed equally to this work as the corresponding authors.

*Correspondence:

Hee Young Na
heeyoungna86@gmail.com
Jaihwon Kim
drjaihwon@snu.ac.kr

Full list of author information is available at the end of the article



© The Author(s) 2025. **Open Access** This article is licensed under a Creative Commons Attribution-NonCommercial-NoDerivatives 4.0 International License, which permits any non-commercial use, sharing, distribution and reproduction in any medium or format, as long as you give appropriate credit to the original author(s) and the source, provide a link to the Creative Commons licence, and indicate if you modified the licensed material. You do not have permission under this licence to share adapted material derived from this article or parts of it. The images or other third party material in this article are included in the article's Creative Commons licence, unless indicated otherwise in a credit line to the material. If material is not included in the article's Creative Commons licence and your intended use is not permitted by statutory regulation or exceeds the permitted use, you will need to obtain permission directly from the copyright holder. To view a copy of this licence, visit <http://creativecommons.org/licenses/by-nc-nd/4.0/>.

Background

Pancreatic ductal adenocarcinoma (PDAC) is the third leading cause of cancer-related deaths, with a discouraging 5-year survival rate of only 12% in the United States [1]. It is treated with neoadjuvant chemotherapy (NAT) and/or radiotherapy; [2] however, it often remains refractory to these treatments [3]. Approximately only 15% of patients present with resectable or borderline resectable PDAC, with surgery followed by chemotherapy as the mainstay of treatment [2]. Although immune checkpoint inhibitors have shown durable clinical benefits in a wide range of malignancies, these benefits have not been significant in PDAC [4], probably because of highly immunosuppressive microenvironment of PDAC [3].

Efforts to enhance therapeutic efficacy have led to ongoing research on prognostic and predictive factors, as well as molecular subtyping of PDAC [5]. However, the current molecular subtyping of PDAC is in its early stages and has not yet influenced clinical management [6, 7]. In the COMPASS trial, the “classical” subtype of PDAC exhibited a favorable response to chemotherapy compared to the “basal-like” subtype [8]. However, owing to numerous limitations in interpretation and application, it is challenging to incorporate these results into clinical practice [5].

Recent advancements in single-cell RNA sequencing and spatial transcriptomics have aimed to overcome the limitations of bulk sequencing [7]. Hwang et al. utilized these techniques to construct a high-resolution molecular landscape of PDAC by refining its molecular and cellular taxonomy [9]. Farren et al. applied digital spatial profiling to PDAC samples, suggesting that actionable signaling and immune biomarkers may shed light on how conventional therapy can be maneuvered to improve its efficacy [10]. Studies investigating the crosstalk between tumor cells and the tumor microenvironment (TME) [11] continue to discover possible druggable targets and prognostic indicators in PDAC [3] as well as other cancers or infectious diseases [12].

This study aimed to discover potential prognostic and predictive factors of PDAC, using digital spatial profiling and immunohistochemistry. We also compared the differentially expressed genes and proportions of immune cell components between PDACs that were treated with upfront surgical resection (UFS) and NAT to investigate the effect of chemotherapy. Additionally, we compared the differences between PDACs based on their response to chemotherapy to find out predictive markers.

Methods

Patients and samples

Forty-eight patients who underwent surgical resection for pancreatic cancer at Seoul National University Bundang Hospital between May 2017 and December 2019

were enrolled. Among these, 24 patients were treated with UFS (UFS group), and 24 underwent neoadjuvant FOLFIRINOX chemotherapy followed by surgery (NAT group). Clinicopathological information, including sex, age, and cancer stage, was retrieved from electronic medical records and pathology reports. Pathological staging was performed according to the eighth edition of the American Joint Committee on Cancer staging manual [13]. The tumor response to NAT was scored based on the College of American Pathologists (CAP) grading system [14]. A CAP score of 0 was defined as a pathologic complete response with no viable residual tumor. A CAP score of 1 was assigned to cases showing near-complete responses with single cells or rare small groups of cancer cells. A CAP score of 2 indicated a partial response with residual cancer and evident tumor regression but more than single cells or rare small groups of cancer cells. A CAP score of 3 was determined in cases of poor or no response, characterized by extensive residual cancer with no evident tumor regression. This study was conducted in accordance with the Declaration of Helsinki and was approved by the Institutional Review Board of Seoul National University Bundang Hospital (no. B-2201-735-301).

Tissue microarray (TMA) construction

A tissue microarray (TMA) was constructed using 2-mm diameter cores derived from formalin-fixed paraffin-embedded blocks after choosing the most representative tumor areas. GeoMx® Digital Spatial Profiler (DSP) (NanoString Technologies Inc., Seattle, WA, USA). Transcriptomic Atlas and IHC analyses were performed in the TMA block.

Spatial transcriptomic analyses

The TMA slides were stained with fluorescently-labeled antibodies directed against pan-cytokeratin (pan-CK) (green), CD45 (red) and alpha-SMA (yellow), which served as visualization markers. The slide was imaged on the GeoMx® platform, which functions in part as a fluorescent slide scanner. One region of interest (ROI) was selected for each TMA core based on the visualization markers using a custom-designed web-based control program. The ROIs were selected such that each component was similarly distributed. Once the ROIs were selected, a programmable digital micromirror device precisely directed ultraviolet light to illuminate each ROI and cleave the oligos in a region-specific manner. The released indexing DNA oligonucleotides were collected by microcapillary aspiration and deposited in individual wells of a microtiter plate. The localized ultraviolet exposure and ultraviolet-cleaved oligo collection were repeated for each ROI.

Library preparation and sequencing

Library preparation was conducted following the protocol provided by NanoString Technologies, specifically the NanoString DSP-Genomics Library Preparation Protocol, as described by Merritt et al. [15]. Oligonucleotides from each ROI were amplified using PCR, employing the i5/i7 dual-indexing system from Illumina to ensure that the identity of each ROI was preserved. The PCR products were combined and cleaned using double-round AMPure XP beads (Beckman Coulter, Brea, CA, USA). A Bioanalyzer High-Sensitivity DNA Chip (Agilent Technologies, Santa Clara, CA, USA) was used to assess the concentration and purity of the prepared library. Sequencing was performed using paired-end reads (2×75 bp) on an Illumina NextSeq system (Illumina Inc. San Diego, CA, USA). The sequencing reads were subsequently aligned to specific analyte barcodes using the Bowtie tool.

Differentially expressed genes and pathway enrichment analysis

Count data were generated from the DSP pipeline and technically pre-processed using the GeoMx® Data Analysis Suite (DSPDA). Differentially expressed gene (DEG) analysis was conducted by integrating sample, group, and ROI annotations using the standR packages [16]. After quality control, the data were normalized using the Trimmed Mean of M-values method, and genes with low coverage were filtered using edgeR::filterByExpr. Differential expression analyses were performed using voom-limma-duplicate correlation with the edgeR::voomLmFit function to fit the linear model. An empirical Bayes-moderated t-statistic was generated, and statistically significant genes were identified based on the criteria of $|\log_2 \text{fold change (FC)}| > 1$ and an adjusted p-value of < 0.05 . The false discovery rate (FDR) was controlled by adjusting the p-value using the Benjamini–Hochberg procedure. Ranking genes by fold change expression and gene set enrichment analysis (GSEA) were performed using clusterProfiler packages [17] for hallmark gene sets and immunologic signatures obtained from the Molecular Signatures Database (MSigDB).

Estimate of infiltrating immune cell subsets

CIBERSORTx is an analytical tool that estimates the relative abundance of specific cell types in bulk tumors based on gene expression profile data [18]. To realize the precise quantification of the fraction of 22 immunocyte types, we used a gene signature matrix consisting of 547 genes, termed “LM22 signature matrix file,” and set the quantity of permutations to 100 and no batch correction with disabled quantile normalization on CIBERSORTx web pages (<https://cibersortx.stanford.edu/>). For each sample, 22 types of immune cells were quantified along with CIBERSORTx metrics, including the Pearson

correlation coefficient, CIBERSORTx p-value, and root mean squared error (RMSE). The statistical significance of the deconvolution results for the entire cellular subgroup was represented by the CIBERSORTx value, which was employed to exclude deconvolutions with less remarkable fit precision.

Immunohistochemical analyses

TMA was sectioned at a thickness of 4-μm and stained with specific antibodies against CD3 (polyclonal, 1:100, Dako, Glostrup, Denmark), CD20 (L26, ready-to-use, Dako), CD4 (SP35, ready-to-use, Ventana Medical Systems, Tucson, AZ, USA), CD8 (C8/144B, ready-to-use, Dako), CD68 (PG-M1, 1:300; Dako), and CD163 (OTI2G12, 1:500, Abcam, Cambridge, UK). Immunostaining was performed using the Ventana BenchMark XT staining system. The open-source software Qupath (<https://qupath.github.io/>) [19] was utilized to quantify each IHC-positive cell. Cell density was calculated as the number of IHC-positive cells per 1 mm², and the median density for each antibody was used as the cutoff for statistical purposes.

Statistical analyses

Pearson's chi-square test or Fisher's exact test was used to compare categorical variables. To compare continuous variables, the independent samples t-test or Mann–Whitney U test was used. Univariate and multivariate logistic regression analyses were performed to determine the clinicopathological features associated with prognosis. Survival outcomes were estimated using Kaplan–Meier analysis and compared using the log-rank test. The clinical factors that affected survival were identified using the Cox proportional hazards model, and hazard ratios (HRs) were calculated using 95% confidence intervals (CIs). The results were considered statistically significant with a two-tailed p-value of less than 0.05. All data were analyzed using SPSS software (version 22.0; IBM Corp., Armonk, NY, USA) and R (version 3.6.3, <http://www.r-project.org/>, accessed on September 10, 2021).

Results

Patient characteristics

The clinicopathological characteristics of patients with PDAC are summarized in Table 1. Despite the higher rates of initial resectability and negative postoperative surgical margins in the UFS group, there were no significant differences in most clinicopathological parameters. Preoperative CA19-9 levels were significantly lower in the NAT group, although there was no significant difference in the initial or postoperative CA 19-9 levels.

Table 1 Clinicopathologic characteristics of patients with pancreatic cancer

	All (N=48)	UFS group (N=24)	NAT group (N=24)	p-value
Sex				0.149
Male	23 (47.9%)	14 (58.3%)	9 (37.5%)	
Female	25 (52.1%)	10 (41.7%)	15 (62.5%)	
Age				0.235
Median (range) (years)	66 (41–84)	67 (41–84)	64 (48–77)	
Initial stage (image)				< 0.001
Resectable	24 (50.0%)	24 (100%)	0 (0%)	
Borderline resectable	20 (41.7%)	0 (0%)	20 (83.3%)	
Locally advanced	3 (6.3%)	0 (0%)	3 (12.5%)	
Metastatic	1 (2.1%)	0 (0%)	1 (4.2%)	
Initial CA 19–9				0.864
Median (range)	149 (6–5800)	187 (8–5800)	131 (6–2549)	
Preoperative CA 19–9				0.014
Median (range)	103 (5–5800)	187 (8–5800)	39 (5–1260)	
Post-op CA 19–9				0.059
Median (range)	56 (5–420)	87 (6–420)	25 (5–201)	
Surgery				0.771
Pancreatoduodenectomy	27 (56.3%)	13 (54.2%)	14 (58.3%)	
Distal pancreatectomy	21 (43.8%)	11 (45.8%)	10 (41.7%)	
Pathologic diagnosis				0.234
Ductal adenocarcinoma	45 (93.8%)	24 (100%)	21 (87.5%)	
Adenosquamous carcinoma	3 (6.3%)	0 (0%)	3 (12.5%)	
Differentiation				0.066
Moderately differentiated	32 (66.7%)	13 (54.2%)	19 (79.2%)	
Poorly differentiated	16 (33.3%)	11 (45.8%)	5 (20.8%)	
Tumor location				0.213
Uncinate process, head, neck	25 (52.1%)	11 (45.8%)	14 (58.3%)	
Body, tail	23 (47.9%)	13 (54.2%)	10 (41.7%)	
Tumor size				0.369
Median (range) (cm)	2.8 (1.0–7.7)	2.9 (1.2–4.7)	2.6 (1.0–7.7)	
Angiolymphatic invasion				0.540
Absent	16 (33.3%)	7 (29.2%)	9 (37.5%)	
Present	32 (66.7%)	17 (70.8%)	15 (62.5%)	
Venous invasion				0.755
Absent	33 (68.8%)	17 (70.8%)	16 (66.7%)	
Present	15 (31.3%)	7 (29.2%)	8 (33.3%)	
Perineural invasion				0.050
Absent	5 (10.4%)	0 (0%)	5 (20.8%)	
Present	43 (89.6%)	24 (100%)	19 (79.2%)	
Surgical margin				0.039
Negative	17 (35.4%)	11 (45.8%)	6 (25%)	
Less than 1 mm	26 (54.2%)	13 (54.2%)	13 (54.2%)	
0 mm	5 (10.4%)	0 (0%)	5 (20.8%)	
pT category				0.245
1–2	40 (83.3%)	22 (91.7%)	18 (75.0%)	
3–4	8 (16.7%)	2 (8.3%)	6 (25.0%)	
pN category				> 0.999
0–1	42 (87.5%)	21 (87.5%)	21 (87.5%)	
2	6 (12.5%)	3 (12.5%)	3 (12.5%)	
Stage (AJCC 8th)				0.401
IA	7 (14.6%)	2 (8.3%)	5 (20.8%)	
IB	9 (18.8%)	4 (16.7%)	5 (20.8%)	
2 A	1 (2.1%)	0 (0%)	1 (4.2%)	

Table 1 (continued)

	All (N= 48)	UFS group (N= 24)	NAT group (N= 24)	p-value
2B	24 (50.0%)	15 (62.5%)	9 (37.5%)	NA
3	7 (14.6%)	3 (12.5%)	4 (16.7%)	
CAP score				
CAP score 2	10 (20.8%)	NA	10 (41.7%)	NA
CAP score 3	14 (29.2%)	NA	14 (58.3%)	

AJCC, american joint committee on cancer; CAP, college of american pathologists; N, number; NA, not applicable; NAT, neoadjuvant chemotherapy; UFS, upfront surgical resection

DEGs and pathway enrichment analysis in the UFS and NAT groups

There were no DEGs between the UFS and NAT groups for any of the three cell types (pan-CK-positive, CD45-positive, or the remaining pan-CK- and CD45-negative cells). In GSEA using hallmark gene sets from MsigDB for pan-CK-positive cells, genes related to the epithelial-mesenchymal transition (EMT) pathway were upregulated in the UFS group, whereas genes related to hypoxia, reactive oxygen species, *MYC* targets, and the *P53* pathway were upregulated in the NAT group (Fig. S1).

DEGs and pathway enrichment analysis in CAP scores 2 and 3 subgroups

There were no DEGs in pan-CK-positive and CD45-positive cells between the two subgroups. However, in the remaining cells, *KRT8* was upregulated in the CAP score 3 subgroup, whereas *MFAP4* and *EGR3* were upregulated in the CAP score 2 subgroup (Fig. 1A). When adjusting the FDR-adjusted p-value cutoff to 0.1, seven mRNAs were upregulated in the CAP score 3 subgroup (*KRT8*, *KRT19*, *SLC2A1*, *ALDOA*, *S100A6*, *S100A10*, and *SPPI*) compared to the CAP score 2 subgroup. Protein-protein interaction analysis using STRING (medium confidence (0.4), maximum number of interactors: 5 (1st shell)) showed that *GAPDH* was the hub node among these genes (Fig. S2). Of note, GSEA using hallmark gene sets in pan-CK-positive cells showed that genes related to the TGF-beta pathway were upregulated in the CAP score 3 subgroup. In contrast, IFN-gamma and alpha response-related gene pathways were enriched in the CAP score 2 subgroup (Fig. 1B). GSEA using immune signature gene sets from CD45-positive cells revealed that genes related to monocyte-associated pathways were enriched in the CAP score 3 subgroup, whereas genes related to B or T cell-associated pathways were enriched in the CAP score 2 subgroup (Fig. 1C). In the remaining cells, GSEA using hallmark genes showed that EMT- and angiogenesis-related pathways were prominent in the CAP score 3 subgroup. IFN-gamma and TNF-alpha pathways were upregulated in the CAP score 2 subgroup (Fig. 1D).

Immune cell composition analysis using CIBERSORT

Deconvolution of CD45-positive cells was performed using CIBERSORTx. When the proportions of immune cells in each case were dichotomized into low or high (cutoff: median), high plasma cell infiltration was more frequently observed in UFS group ($p=0.013$) (Fig. 2A). High CD8 T cell, CD4 naïve T cell, CD4 memory resting T cell and CD4 memory active T cell infiltration were more common in CAP score 2 group, but the differences were not statistically significant.

High CD8 T cell infiltration was associated with lower postoperative CA19-9 levels (cutoff: median) and negative surgical margins (all $p<0.05$). High naïve B-cell infiltration was also associated with favorable clinico-pathological variables, including lower initial and postoperative CA19-9 levels, absence of venous invasion, and lower recurrence rates (all $p<0.05$). In contrast, high monocyte infiltration was associated with higher frequencies of recurrence ($p=0.018$) and death ($p=0.006$) (Table S1).

Immune cell composition analysis using immunohistochemistry

Representative IHC images for each antibody and immune cell densities are presented in Fig. S3 and Table S2. In the NAT group, high CD3-, CD4-, CD8-, and CD163-positive cell infiltrations were more frequent in the CAP 2 subgroup than in the CAP 3 subgroup (all $p<0.05$) (Table 2).

High CD3-, CD4-, and CD8-positive cell infiltrations were associated with a lower pT category and a lower frequency of recurrence (all $p<0.05$). In addition, high CD3- and CD4-positive cell infiltrations were associated with the absence of venous invasion ($p=0.029$). High CD8-positive cell infiltration was associated with lower initial CA19-9 levels ($p=0.019$). (Supplementary Table S3).

Survival analysis

At the time of analysis, the median progression-free survival (PFS) and overall survival (OS) were 15.9 months (range, 4.0–76.9) and 33.7 months (range, 5.0–86.5), respectively. Thirty-five patients (72.9%) had disease progression, and 36 (75.0%) died. In the multivariate Cox regression analysis for OS, three variables remained

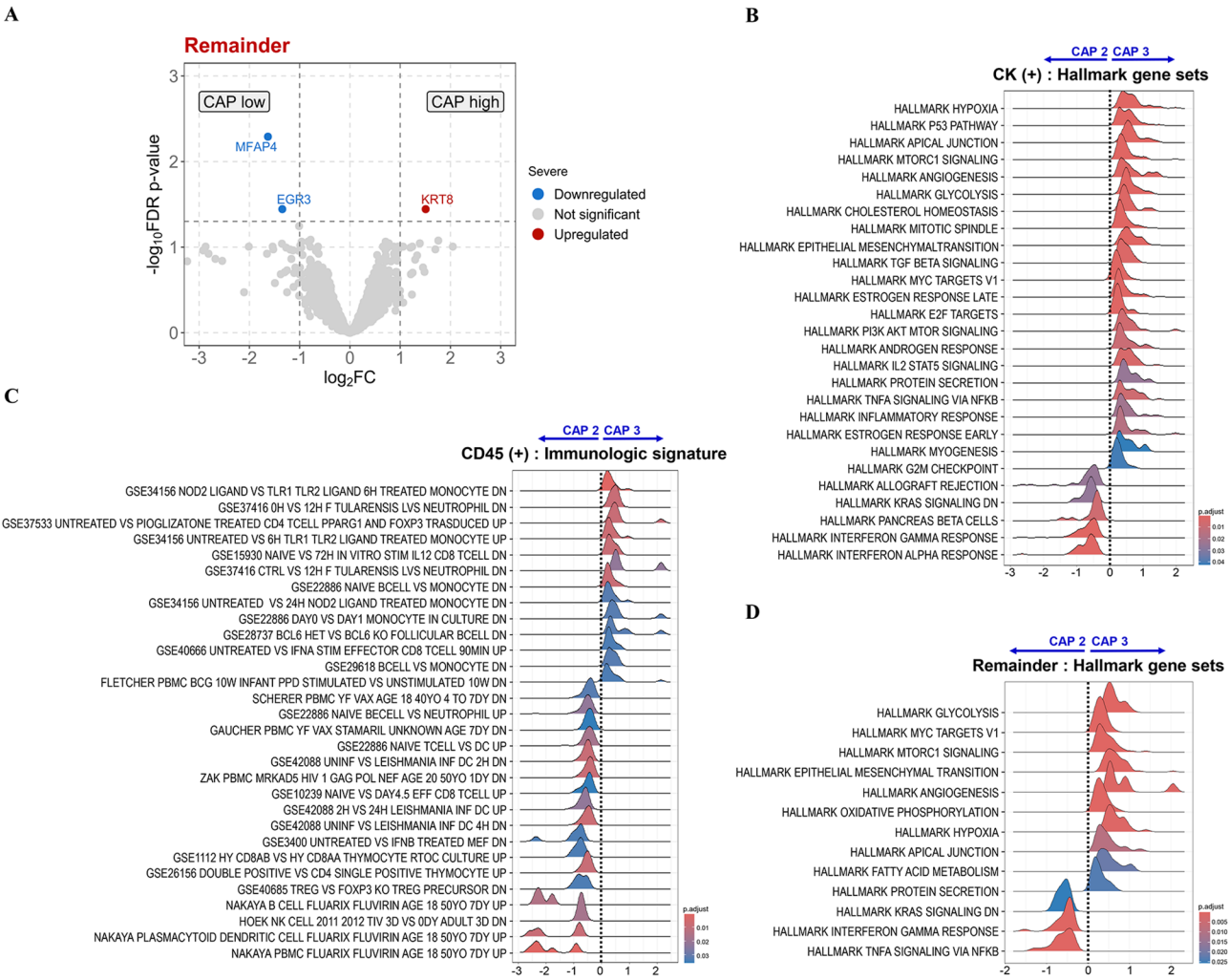


Fig. 1 Differences in gene expression between the CAP subgroups in the neoadjuvant chemotherapy group. **(A)**, Volcano plot depicting differentially expressed genes in the CAP scores 2 and 3 subgroups in the remainder cells. The p-values represent a function of the fold change (FC) between the indicated groups. The cutoff used was: $|\log_2FC| > 1$ and FDR-adjusted p-value < 0.05 . Red dots indicate significantly upregulated genes, and blue dots indicate significantly downregulated genes in the CAP score 3 subgroup compared with the CAP score 2 subgroup. **(B)**, Gene set enrichment analysis (GSEA) using hallmark gene sets from MSigDB in the pan-CK-positive cells showed that genes related to the TGF-beta pathway were upregulated in the CAP score 3 subgroup. However, IFN-gamma and alpha response-related gene pathways were enriched in the CAP score 2 subgroup. **(C)**, GSEA using immune signature gene sets from MSigDB in CD45-positive cells revealed that genes related to monocyte-associated pathways were enriched in the CAP score 3 subgroup, and genes related to B or T cell-associated pathways were enriched in the CAP score 2 subgroup. **(D)**, GSEA using hallmark gene sets from MSigDB in the remaining cells showed that EMT and the angiogenesis-related pathways were prominent in the CAP score 3 subgroup. However, IFN-gamma and TNF-alpha pathways were upregulated in the CAP score 2 subgroup.

independent prognostic factors: age, high monocyte infiltration, and high CD68-positive cell infiltration. For PFS, the multivariate analysis revealed female sex, high post-operative CA19-9 level, and high monocyte infiltration as independent prognostic factors (Table 3). In the Kaplan–Meier survival analysis, high monocyte infiltration and high CD68-positive cell infiltration were associated with longer OS (all $p < 0.05$) (Fig. 3). There was a trend toward improved PFS for high CD3-, CD4-, and CD8-positive cell infiltration, which was not statistically significant (Fig. S4).

In the UFS group, only high monocyte infiltration was associated with worse OS in the univariate analysis ($p = 0.017$). Venous invasion and high monocyte infiltration were independent prognostic factors for PFS in the multivariate analysis (Supplementary Table S4). In the NAT group, high plasma cell infiltration and high M0 macrophage infiltration remained independent prognostic factors for OS. Multivariate analysis for PFS identified CAP score 3 and high plasma cell infiltration as independent prognostic factors (Table S5).

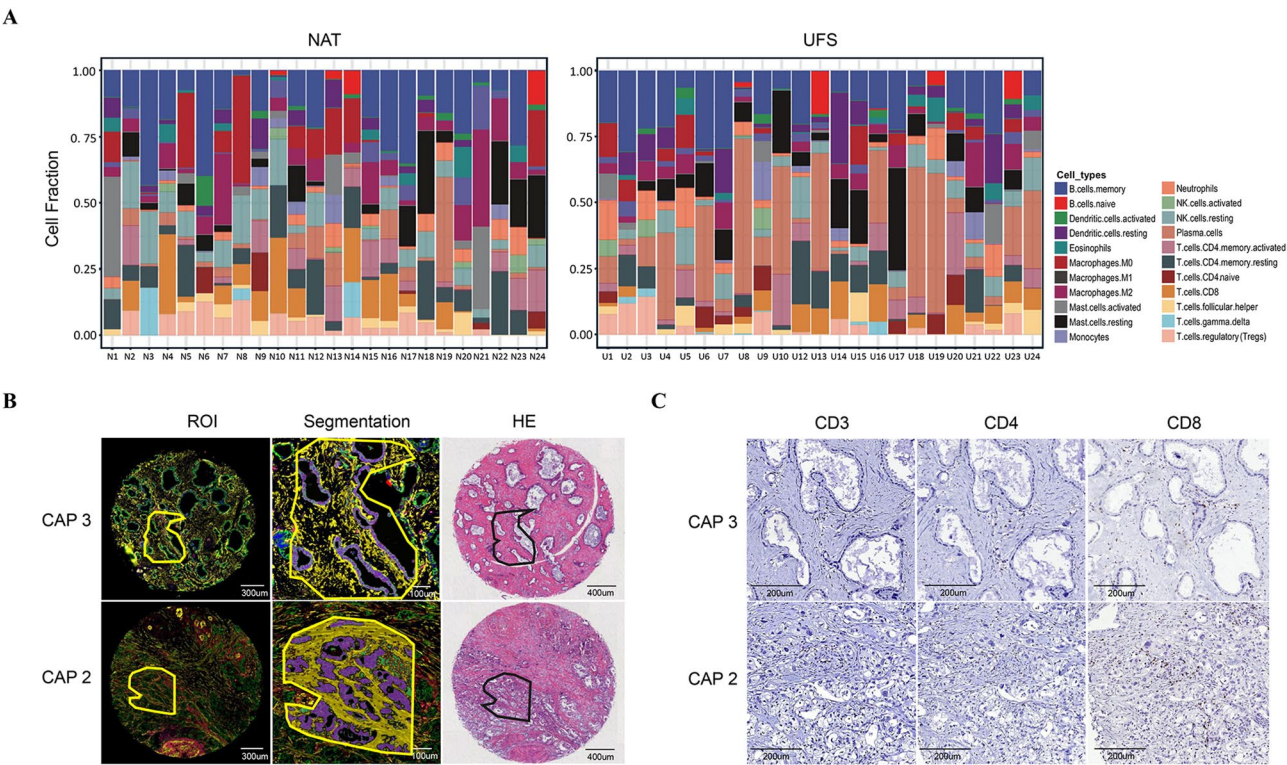


Fig. 2 Immune cell deconvolution analysis using CIBERSORTx and immunohistochemical analysis. **(A)**, High plasma cell infiltration was more common in upfront surgery (UFS) group. **(B)**, After each region of interest (ROI) per one core, which is composed of three cell components, was selected (pan-CK: green, CD45: red, alpha-SMA: yellow) from CAP 3 and CAP 2 subgroup, segmentation was performed for sequencing (pan-CK: magenta, CD45: green, the remaining cells: yellow). Higher proportion of CD45 cell in CAP 2 than in CAP3 is noted. Black contour in HE stained cores match with the ROIs. **(C)** CD3, CD4, CD8 immunohistochemistry revealed higher CD3, CD4 and CD8-positive cell infiltration in CAP2

Table 2 Results of immunohistochemical analysis in pancreatic cancer

IHC antibody	UFS group	NAT group	p-value	NAT group		p-value
				CAP score 2	CAP score 3	
	(N = 24)	(N = 24)		(N = 10)	(N = 14)	
CD3 IHC			1.000			0.036
Low	12 (50.0%)	12 (50.0%)		2 (20.0%)	10 (71.4%)	
High	12 (50.0%)	12 (50.0%)		8 (80.0%)	4 (28.6%)	
CD4 IHC			0.564			0.005
Low	13 (54.2%)	11 (45.8%)		1 (10.0%)	10 (71.4%)	
High	11 (45.8%)	13 (54.2%)		9 (90.0%)	4 (28.6%)	
CD8 IHC			1.000			0.036
Low	12 (50.0%)	12 (50.0%)		2 (20.0%)	10 (71.4%)	
High	12 (50.0%)	12 (50.0%)		8 (80.0%)	4 (28.6%)	
CD20 IHC			0.564			0.240
Low	13 (54.2%)	11 (45.8%)		3 (30.0%)	8 (57.1%)	
High	11 (45.8%)	13 (54.2%)		7 (70.0%)	6 (42.9%)	
CD68 IHC			0.083			0.403
Low	9 (37.5%)	15 (62.5%)		5 (50.0%)	10 (71.4%)	
High	15 (62.5%)	9 (37.5%)		5 (50.0%)	4 (28.6%)	
CD163 IHC			0.021			0.032
Low	8 (33.3%)	16 (66.7%)		4 (40.0%)	12 (85.7%)	
High	16 (66.7%)	8 (33.3%)		6 (60.0%)	2 (14.3%)	

CAP, college of american pathologists; IHC, Immunohistochemical analysis; N, number; NAT, neoadjuvant chemotherapy; UFS, upfront surgical resection

Table 3 Multivariate analysis for overall survival and progression free survival in all cases

Variables	Overall survival				Progression free survival				
	Univariate		Multivariate		Univariate		Multivariate		
	HR	95% CI	p-value	HR	95% CI	p-value	HR	95% CI	p-value
Clinicopathologic factors									
Age (continuous)	1.046	1.004–1.091	0.033	1.048	1.006–1.093	0.025	1.028	0.987–1.071	0.179
Sex (Female)	1.57	0.809–3.046	0.183				2.02	1.023–3.988	0.043
NAT	0.852	0.442–1.643	0.633				0.723	0.372–1.406	0.339
pT category (3–4)	1.696	0.736–3.906	0.215				2.319	1.016–5.292	0.046
pN category (2)	2.244	0.925–5.446	0.074				3.144	1.263–7.822	0.014
Differentiation (PD)	1.293	0.642–2.606	0.471				1.684	0.844–3.361	0.139
Surgical RM positive (< 1 mm)	1.003	0.507–1.984	0.992				1.055	0.525–2.122	0.88
Angiolymphatic invasion	1.653	0.810–3.375	0.167				3.128	1.405–6.964	0.005
Venous invasion	0.994	0.493–2.003	0.986				1.338	0.663–2.699	0.416
Perineural invasion	2.689	0.643–11.245	0.175				3.213	0.764–13.504	0.111
Initial CA19-9 ≥ median	1.309	0.638–2.686	0.463				1.698	0.807–3.575	0.163
Postop CA19-9 ≥ median	1.506	0.741–3.058	0.258				2.19	1.047–4.583	0.037
DSP immune cell fraction status									
CD8 T cells high	1.359	0.699–2.642	0.366				1.113	0.567–2.186	0.755
CD4 naive T cells high	1.129	0.552–2.307	0.74				0.778	0.362–1.671	0.52
Naive B cells high	0.671	0.259–1.739	0.411				0.313	0.095–1.030	0.056
Plasma cell high	1.678	0.856–3.292	0.132				1.592	0.802–3.161	0.184
Monocytes high	2.456	1.228–4.9141	0.011	2.601	1.290–5.244	0.008	2.088	1.040–4.194	0.038
Memory B cells high	1.62	0.822–3.196	0.164				1.556	0.784–3.091	0.206
Memory resting CD4 T cells high	1.178	0.606–2.289	0.63				1.253	0.638–2.463	0.513
Memory activated CD4 T cells high	0.766	0.394–1.489	0.431				0.651	0.331–1.283	0.215
Follicular helper T cells high	2.512	0.332–19.041	0.373				8.586	1.003–73.512	0.05
Regulatory T cells high	0.672	0.344–1.311	0.244				0.836	0.426–1.641	0.603
Gamma delta T cells high	0.638	0.264–1.541	0.318				0.757	0.313–1.830	0.536
Resting NK cells high	0.808	0.415–1.573	0.53				0.862	0.439–1.693	0.666
Activated NK cells high	0.624	0.271–1.436	0.267				0.959	0.433–2.125	0.918
M0 macrophages high	0.609	0.313–1.186	0.145				0.72	0.366–1.417	0.342
M1 macrophages high	1.05	0.541–2.038	0.886				1.316	0.670–2.586	0.426
M2 macrophages high	0.882	0.454–1.713	0.711				1.131	0.574–2.229	0.722
Resting dendritic cells high	1.198	0.611–2.349	0.6				1.296	0.652–2.575	0.459
Activated dendritic cells high	1.139	0.585–2.216	0.702				1.296	0.658–2.552	0.453
Resting mast cells high	1.161	0.596–2.259	0.661				1.085	0.551–2.135	0.813
Activated mast cells high	1.219	0.623–2.387	0.563				1.482	0.750–2.927	0.258
Eosinophils high	0.841	0.430–1.645	0.613				0.664	0.331–1.329	0.247
Neutrophils high	0.735	0.377–1.431	0.365				1.036	0.528–2.034	0.918
IHC immune cell density status									

Table 3 (continued)

Variables	Overall survival				Progression free survival			
	Univariate		Multivariate		Univariate		Multivariate	
	HR	95% CI	p-value		HR	95% CI	p-value	
CD3 IHC high	0.806	0.417–1.561	0.523		0.603	0.302–1.200	0.15	
CD4 IHC high	0.782	0.405–1.511	0.465		0.566	0.285–1.122	0.103	
CD8 IHC high	0.693	0.355–1.353	0.283		0.512	0.254–1.031	0.061	
CD20 IHC high	1.298	0.669–2.518	0.44		1.119	0.576–2.175	0.741	
CD68 IHC high	2.255	1.133–4.489	0.021	2.255	1.409	0.724–2.742	0.313	
CD163 IHC high	0.71	0.367–1.374	0.309		0.609	0.308–1.202	0.153	

DSP, Digital spatial profiling; NAT, neoadjuvant chemotherapy; PD, poorly differentiated; RM, resection margin

Discussion

This study aimed to investigate the differences between the UFS and NAT groups and the CAP scores 2 and 3 groups using DSP and IHC analysis. Although there were no significant differences in RNA expression between the UFS and NAT groups, subgroup analysis based on NAT response revealed that the differences in RNA expression mainly occurred in the tumor stroma. When examining the immune cell fraction through cell deconvolution analysis, the differences between each group were not prominent; however, a high monocyte status was identified as an independent poor prognostic factor for both OS and PFS in patients with PDAC, suggesting its potential as a prognostic predictor. IHC revealed that high CD3-, CD4-, and CD8-positive cell infiltration was significantly associated with a better NAT response. In addition, high CD68-positive cell infiltration was an independent prognostic factor for OS, which was consistent with the DSP results.

The absence of DEGs between the UFS and NAT groups suggested that NAT did not alter the overall RNA expression profiles in PDAC. Similarly, Farren et al. conducted RNA sequencing to assess the effect of NAT on gene expression patterns related to immunological function in PDAC tumors and reported no DEGs between the two groups [10]. A study that analyzed the effects of chemotherapy on PDAC using single-cell RNA sequencing also demonstrated that chemotherapy did not induce significant changes in tumor subtype composition and that intertumoral heterogeneity was highly pronounced [20]. Additionally, the study demonstrated that chemotherapy did not significantly alter the subpopulations of cancer-associated fibroblasts and macrophages within the tumor microenvironment (TME) [20], aligning with the findings of this study. However, Porter et al. addressed that that FOLFIRINOX combination chemotherapy in pancreatic cancer induces a more quasi-mesenchymal state [21]. Further studies including matched pre- and post- chemotherapy samples are necessary to assess the precise role of chemotherapy in PDAC.

Within the NAT group, subgroup analysis based on the CAP score revealed differential gene expression patterns only in pan-CK- and CD45-negative remaining cells, suggesting the role of the tumor stroma in determining treatment responses. *MFAP4* and *EGR3* were significantly upregulated in the CAP score 2 subgroup compared with the CAP score 3 subgroup. Although the role of *MFAP4* in malignancy is not clearly understood, it is known to be strongly associated with the impairment and alteration of elastic fibers and the mechanism of fibrogenesis [22, 23]. High mRNA expression of *MFAP4* was significantly correlated with improved survival outcome in breast cancer [23], lung adenocarcinoma [24] and oral squamous cell carcinoma [25]. Similarly, Li et al. found that patients

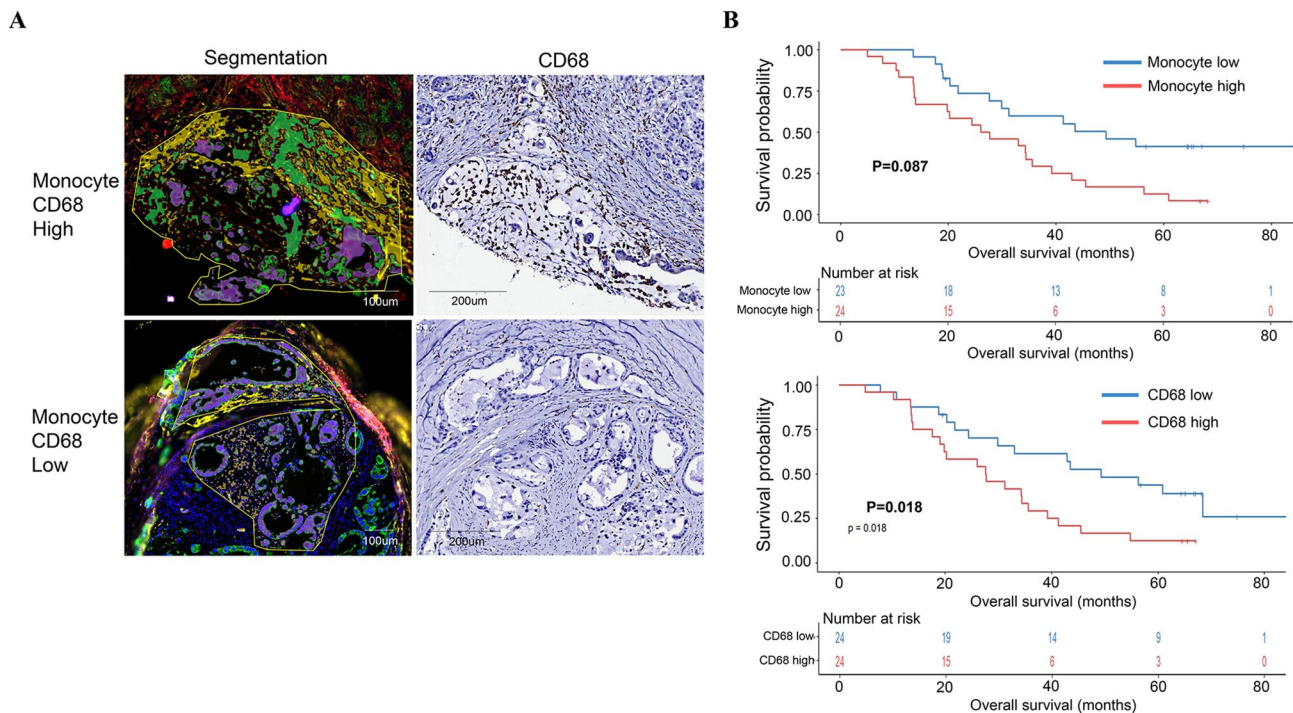


Fig. 3 Representative images of fluorescent and CD68 immunohistochemical staining and Kaplan-Meier survival curves. **(A)**, Representative cases showing high and low monocyte and CD68-positive cell infiltration. **(B)**, Kaplan-Meier survival analysis reveals significantly poor overall survival in high monocyte and CD68-positive cell infiltration cases

with hepatocellular carcinoma (HCC) with higher MFAP4 protein and mRNA expression in peritumoral stromal tissues had a longer OS, potentially due to its role in maintaining extracellular matrix integrity and promoting immune cell infiltration [26]. Based on these observations, we propose that *MFAP4* plays a critical role in modulating the tumor microenvironment by promoting immune cell infiltration, which may in turn enhance the efficacy of chemotherapy. This is further supported by our findings, where the CAP 2 subgroup, characterized by high *MFAP4* expression, also exhibited increased infiltration of CD3-, CD4-, and CD8-positive T cells. These findings suggest that *MFAP4* may play a role in shaping an immune-permissive tumor microenvironment, potentially explaining the improved NAT response observed in these patients. Conversely, in serous ovarian cancer [27] and neuroblastoma [28], high *MFAP4* expression was associated with inferior survival. In gliomas, *MFAP4* is aberrantly overexpressed and has been associated with adverse clinicopathological features [29]. While this finding contrasts with our results, it is notable that high *MFAP4* expression in gliomas is also linked to increased T cell infiltration [29], which aligns with our data. To date, few studies have investigated the role of *MFAP4* in PDAC. Further studies, including functional analyses of *MFAP4*, are warranted to clarify its precise role in PDAC.

Although *EGR3* regulates neurodevelopment [30], autoimmunity [31], inflammation [32], and angiogenesis

[33], its role in tumorigenesis remains controversial. High *EGR3* expression is associated with poor survival in breast cancer [34, 35], adrenal cortical carcinoma [36] and glioblastoma [37]. In contrast, an association between decreased *EGR3* expression and poor survival has been observed in gastric cancer [38] and cutaneous melanoma [36]. Shin et al. also revealed that *EGR3* blocks the EMT process and suppresses tumor migration and invasion by transcriptionally activating *ZFP36*, *GADD45B* and *SOC3* genes in prostate cancer [39]. These latter results align with the pathway analysis in our study, which revealed highly enriched EMT-related pathways in the CAP 3 subgroup compared with the CAP score 2 subgroup. Moreover, a recent study using The Cancer Genome Atlas pan-cancer data reported that *EGR3* mRNA expression was associated with high immune cell infiltration [36]. Additionally, another study found that the transcription factors *EGR2* and *EGR3* were highly induced in tumor-infiltrating lymphocytes (TILs) across multiple cancer patient cohorts. The deficiency of *EGR2* and *EGR3* in T cells resulted in enhanced tumor growth and fewer TILs in mouse models [40], which may explain the higher density of CD3-, CD4-, and CD8-positive immune cells in the CAP score 2 subgroup in this study. High expression of *MFAP4* and *EGR3* is a potential predictive marker for the NAT response in PDAC. Patients exhibiting low levels of these markers, if this can be screened in routine practice [41], may benefit

less from NAT and might be more appropriately managed with alternative strategies—such as radiation therapy or targeted treatments tailored to their mutational profiles—alongside conventional chemotherapy. This might ultimately lead to our understanding of PDAC and improved prognosis in PDAC [42]. Nonetheless, validation in large independent cohort using single cell RNA sequencing or multi-region spatial profiling, especially focusing on the various components of tumor microenvironment, as well as preclinical studies using cell line or patient-derived xenograft model, are warranted.

KRT8 was upregulated in the non-epithelial, non-immune cell compartment of the CAP score 3 subgroup. Although KRT8 is normally expressed in epithelial cells, including pancreatic acinar and ductal cells [43], Shi et al. reported that increased c-Myc expression in fibroblasts resulted in increased and decreased expression of epithelial and mesenchymal markers, respectively, thereby leading to mesenchymal-epithelial transition (MET) [44]. Although the precise mechanism by which fibroblasts in PDAC express KRT8 remains unclear, our results suggest that *KRT8* expression in stromal cells is a possible predictive marker for NAT. In addition, when adjusting the FDR-adjusted p-value cutoff to 0.1, protein-protein interaction analysis showed that *GAPDH* was the hub node of upregulated genes in the CAP score 3 subgroup. *GAPDH* mainly plays a role in glycolysis. Although the role of glycolysis in response to chemotherapy has been scarcely reported, many studies have found that glycolysis promotes tumor growth, metastasis, and chemoresistance and inhibits the apoptosis of tumor cells [45].

The immune cell deconvolution and pathway analysis results from the DSP data correlated well with the IHC results. In the CAP score 2 subgroup, in which B and T cell-associated pathways were enriched, high CD3-, CD4- and CD8-positive cell infiltration was noted in IHC. In the CAP score 3 subgroup, genes related to the TGF-beta pathway, which is known to create an immune-suppressive tumor microenvironment and tumor progression [46, 47], were upregulated in pan-CK-positive cells. These results also correlated well with the low immune cell infiltration and limited chemotherapy response in the CAP 3 subgroup. Although a higher density of TILs has been reported to be associated with better prognosis in PDAC [48], limited data are available regarding the predictive role of TIL in NAT response. This study proposes the possible utility of CD3, CD4, and CD8 IHC as predictive markers for the NAT response, although additional research is required.

In the survival analysis, high monocyte infiltration was found to be an independent poor prognostic factor for OS and PFS overall and in the UFS group. These results align with previous studies in which most types of cancer, including lung cancer, breast cancer, HCC and gastric

cancer, high levels of tumor-associated macrophages in the TME were associated with cancer progression, metastatic spread, poor treatment efficacy and shorter survival time [49]. When multivariate analysis was performed separately, high CD68-positive cell infiltration was also found to be an independent prognostic factor for OS, confirming the DSP results. Although statistical significance was not reached, high CD3-, CD4- and CD8-positive cell infiltration showed a trend toward superior PFS. They were associated with a lower frequency of recurrence. The absence of a statistically significant association may be due to the limited number of patients included in our study, considering that CD3-, CD8-, CD4- positive TILs are associated with prognostic benefits in most cancer types [50].

In the NAT group, high plasma cell infiltration, but not high monocyte infiltration, was an independent poor prognostic factor for OS and PFS. Contrary to our findings, high plasma cell infiltration is generally associated with better outcomes [51, 52]. Plasma cells induce tumor cell death via IgG-mediated antibody-dependent cellular cytotoxicity and promote antigen presentation by dendritic cells [53, 54]. However, sustained antibody production can also promote cancer development and progression by inducing chronic inflammation via immune complexes and an activated complement system, which could explain our results [55]. Furthermore, a recent study employing single-cell multi-omics for a comprehensive analysis of immune cell features in PDAC classified the TME into myeloid-enriched (ME) tumors and adaptive-enriched (AE) tumors [56]. ME tumors, which are characterized by a high density of immunosuppressive myeloid cells, such as macrophages, exhibited higher plasma cell infiltration than AE tumors and were associated with a worse prognosis [56]. These findings are in line with our findings that high plasma cell infiltration in the NAT group was a poor prognostic factor. Although further validation in independent cohorts is required, our results suggest that high plasma cell infiltration may represent an immunosuppressive TME.

A high M0 macrophage infiltration was an independent prognostic factor for improved OS in the NAT group. M0 macrophages can differentiate into M1 and M2 macrophages [57]. Although previous studies have reported that M0 macrophages express M2 macrophage markers [58, 59], the prognostic significance of M0 macrophages in cancer remains contradictory [57, 60, 61]. Therefore, additional research is warranted to determine the role of M0 macrophages in PDAC progression.

This study had some limitations. First, while we carefully selected ROIs for DSP to include the most representative tumor areas, the use of TMA might have not fully capture the intratumoral heterogeneity of the entire tumor. Despite selecting representative regions, spatial

variation within the tumor may limit the generalizability of our findings. Second, the DSP sequencing results were not generated at the single-cell level, limiting our ability to resolve distinct cellular subpopulations. Third, the relatively small sample size reduces the statistical power of subgroup analyses. Fourth, although we analyzed post-operative samples from both the UFS and NAT groups, the absence of matched pre-treatment biopsy samples in NAT group restricts our ability to differentiate chemotherapy-induced effects from baseline tumor heterogeneity. Future studies should incorporate larger, independent cohorts with paired pre- and post-treatment specimens, as well as preclinical models with genetic lineage tracing and single-cell RNA sequencing.

Conclusions

In conclusion, while the gene expression and immune cell infiltration pattern of PDAC appeared largely unaffected by NAT, differences were observed primarily in the tumor stroma and immune cell components between the CAP score 2 and 3 subgroups. *MFAP4*, *EGR3* and *KRT8* expression and CD3, CD4, and CD8 IHC could be possible predictive indicators for NAT. Moreover, high monocyte infiltration and high CD68-positive cell infiltration can be potential prognostic markers in PDAC.

Abbreviations

PDAC	Pancreatic ductal adenocarcinoma
UFS	Upfront surgery
NAT	Neoadjuvant chemotherapy
DSP	Digital spatial profiling
IHC	Immunohistochemical
CAP	College of American Pathologists
TME	Tumor microenvironment
TMA	Tissue microarray
Pan-CK	Pan-cytokeratin
ROI	Region of interest
DEG	Differentially expressed gene
FC	Fold change
FDR	False discovery rate
GSEA	Gene set enrichment analysis
MSigDB	Molecular Signatures Database
CI	Confidence interval
EMT	Epithelial-mesenchymal transition
PFS	Progression-free survival
OS	Overall survival
HCC	Hepatocellular carcinoma
MET	Mesenchymal-epithelial transition
TIL	Tumor infiltrating lymphocyte

Supplementary Information

The online version contains supplementary material available at <https://doi.org/10.1186/s12967-025-06599-9>.

Supplementary Material 1: Table S1: Association of immune cell fraction (DSP) group with various clinicopathologic parameters. Table S2: The result of immunohistochemically positive immune cell density analysis using Qupath. Table S3: Association of immune cell density (IHC) group with various clinicopathologic parameters. Table S4: Multivariate analysis for overall survival and progression free survival in upfront surgery (UFS) group. Table S5: Multivariate analysis for overall survival and progression free survival in neoadjuvant chemotherapy (NAT) group. Fig. S1 Gene set

enrichment analysis using hallmark gene sets from MsigDB in pan-CK-positive cells between the upfront surgical resection group and neoadjuvant chemotherapy groups. Fig. S2 Differentially expressed genes between CAP score 2 and 3 subgroups in the NAT group. Fig. S3 Representative images of immunohistochemical analysis. Fig. S4 Kaplan-Meier survival analysis in all cases.

Acknowledgements

Not applicable.

Author contributions

Y.H., G.L., S.L. and H.N. wrote the manuscript. S.L. and J.O.L. performed differentially expressed genes, pathway enrichment analysis and CIBERSORT analysis. Y.H., S.J., K.L. performed statistical analysis. Y.H., G.L., S.J., S.A. and H.N. performed histologic examination. K.J., J.C.L., Y.Y., J.H., H.H. and J.K. collected, analyzed and interpreted the clinical data. Y.Y., J.H. and H.H. contributed in supervision and resources. H. N. and J.K. were major contributors in conceptualization, review and editing of the manuscript. All authors approved the content of the manuscript and agreed to its publication.

Funding

This study was supported by a grant from the SNUBH Research Fund (No. 14-2019-0029) and a National Research Foundation of Korea (NRF) grant funded by the Korean government (MSIT) (No. 2021R1F1A1062369).

Data availability

The data that support the findings of this study are available from the corresponding author upon reasonable request.

Declarations

Ethics approval and consent to participate

This study was conducted in accordance with the Declaration of Helsinki and was approved by the Institutional Review Board of Seoul National University Bundang Hospital (no. B-2201-735-301).

Consent for publication

All authors have reviewed the final version of the manuscript and approved it for publication.

Competing interests

The authors declared no competing interests that could potentially influence or bias the outcomes of this research.

Author details

- ¹Department of Pathology and Translational Medicine, Seoul National University Bundang Hospital, 82, Fumi-ro 173 Beon-gil, Bundang-gu, Seongnam 13620, Gyeonggi, Republic of Korea
- ²Department of Pathology, Seoul National University College of Medicine, 101, Daehak-ro, Jongno-gu, Seoul 03080, Republic of Korea
- ³Precision Medicine Center, Seoul National University Bundang Hospital, Seongnam 13620, Republic of Korea
- ⁴Department of Health Science and Technology, Graduate School of Convergence Science and Technology, Seoul National University, Seoul 08826, Republic of Korea
- ⁵Department of Pathology, Green Cross Laboratories, Yongin 16924, Republic of Korea
- ⁶Department of Pathology and Translational Genomics, Samsung Medical Center, Sungkyunkwan University School of Medicine, Seoul 03181, Republic of Korea
- ⁷Department of Internal Medicine, Seoul National University Bundang Hospital, 82, Gumi-ro 173 Beon-gil, Bundang-gu, Seongnam 13620, Gyeonggi, Republic of Korea
- ⁸Department of Internal Medicine, Seoul National University College of Medicine, Seoul 03080, Republic of Korea
- ⁹Department of Surgery, Seoul National University Bundang Hospital, Seongnam 13620, Republic of Korea

Received: 9 October 2024 / Accepted: 9 May 2025

Published online: 23 May 2025

References

1. Siegel RL, Miller KD, Wagle NS, Jemal A. Cancer statistics, 2023. *CA Cancer J Clin.* 2023;73(1):17–48.
2. Versteijne EA-O, van Dam JA-O, Suker MA-O, Janssen QP, Groothuis K, Akkermans-Vogelaar JA-O et al. Neoadjuvant chemoradiotherapy versus upfront surgery for resectable and borderline resectable pancreatic cancer: Long-Term results of the Dutch randomized PREOPANC trial. (1527–7755 (Electronic)).
3. Mizrahi JD, Surana R, Valle JW, Shroff RT. Pancreatic cancer. *Lancet.* 2020;395(10242):2008–20.
4. O'Reilly EM, Oh D-Y, Dhani N, Renouf DJ, Lee MA, Sun W, et al. Durvalumab with or without Tremelimumab for patients with metastatic pancreatic ductal adenocarcinoma: A phase 2 randomized clinical trial. *JAMA Oncol.* 2019;5(10):1431–8.
5. Dell'Aquila E, Fulgenzi CAM, Minelli A, Citarella F, Stellato M, Pantano F et al. Prognostic and predictive factors in pancreatic cancer. (1949–2553 (Electronic)).
6. Collisson EA, Bailey P, Chang DK, Biankin AA-O. Mol Subtypes Pancreat cancer. (1759–5053 (Electronic)).
7. Guo JA, Hoffman HI, Weekes CD, Zheng L, Ting DT, Hwang WA-O. Refining the molecular framework for pancreatic Cancer with Single-cell and Spatial technologies. (1557–3265 (Electronic)).
8. Aung KL, Fischer SE, Denroche RE, Jang G-H, Dodd A, Creighton S, et al. Genomics-Driven precision medicine for advanced pancreatic cancer: early results from the COMPASS trial. *Clin Cancer Res.* 2018;24(6):1344–54.
9. Hwang WL, Jagadeesh KA, Guo JA, Hoffman HI, Yadollahpour P, Reeves JW, et al. Single-nucleus and Spatial transcriptome profiling of pancreatic cancer identifies multicellular dynamics associated with neoadjuvant treatment. *Nat Genet.* 2022;54(8):1178–91.
10. Farren MR, Sayegh L, Ware MB, Chen HR, Gong J, Liang Y et al. Immunologic alterations in the pancreatic cancer microenvironment of patients treated with neoadjuvant chemotherapy and radiotherapy. *JCI Insight.* 2020;5(1).
11. Aghapour SA, Torabizadeh M, Bahreiny SS, Saki N, Far MAJ, Yousefi-Avarvand A, et al. Investigating the dynamic interplay between cellular immunity and tumor cells in the fight against cancer: an updated comprehensive review Iranian. *J Blood Cancer.* 2024;16(2):84–101.
12. Aghaei M, Khademi R, Far MAJ, Bahreiny SS, Mahdizade AH, Amirrajab N. Genetic variants of dectin-1 and their antifungal immunity impact in hematologic malignancies: A comprehensive systematic review. *Curr Res Transl Med.* 2024;72(4):103460.
13. AJCC Cancer Staging Manual. 8th ed: Springer Cham; 2016 08 November 2016. XVII, 1032 p.
14. KaKar S, Shi C, Adsay N, Fitzgibbons P, Frankel W, Klistra D, et al. Protocol for the examination of specimens from patients with carcinoma of the pancreas. Northfield, IL: College of American Pathologists (CAP); 2017.
15. Merritt CR, Ong GT, Church SE, Barker K, Danaher P, Geiss G, et al. Multiplex digital Spatial profiling of proteins and RNA in fixed tissue. *Nat Biotechnol.* 2020;38(5):586–99.
16. Liu N, Bhuva DD, Mohamed A, Bokelund M, Kulasinghe A, Tan CW, et al. StandR: Spatial transcriptomic analysis for GeoMx DSP data. *Nucleic Acids Res.* 2024;52(1):e2.
17. Wu T, Hu E, Xu S, Chen M, Guo P, Dai Z, et al. ClusterProfiler 4.0: A universal enrichment tool for interpreting omics data. *Innov (Camb).* 2021;2(3):100141.
18. Newman AA-O, Steen CB, Liu CL, Gentles AA-O, Chaudhuri AA, Scherer F et al. Determining cell type abundance and expression from bulk tissues with digital cytometry. (1546–696 (Electronic)).
19. Bankhead P, Loughrey MB, Fernandez JA, Dombrowski Y, McArt DG, Dunne PD, et al. QuPath: open source software for digital pathology image analysis. *Sci Rep.* 2017;7(1):16878.
20. Werba G, Weissinger D, Kawaler EA, Zhao E, Kalfakakou D, Dhara S, et al. Single-cell RNA sequencing reveals the effects of chemotherapy on human pancreatic adenocarcinoma and its tumor microenvironment. *Nat Commun.* 2023;14(1):797.
21. Porter RL, Magnus NKC, Thapar V, Morris R, Szabolcs A, Neyaz A, et al. Epithelial to mesenchymal plasticity and differential response to therapies in pancreatic ductal adenocarcinoma. *Proc Natl Acad Sci USA.* 2019;116(52):26835–45.
22. Wulf-Johansson H, Lock Johansson S, Schlosser A, Trommelholt Holm A, Melholt Rasmussen L, Mickley H, et al. Localization of Microfibrillar-Associated protein 4 (MFAP4) in human tissues: clinical evaluation of serum MFAP4 and its association with various cardiovascular conditions. *PLoS ONE.* 2013;8(12):e82243.
23. Yang J, Song H, Chen L, Cao K, Zhang Y, Li Y et al. Integrated analysis of microfibrillar-associated proteins reveals MFAP4 as a novel biomarker in human cancers. (1750–192X (Electronic)).
24. Lv R, Wang Y, Lin B, Peng X, Liu J, Lu WD, et al. Targeted luminescent probes for precise Upconversion/NIR II luminescence diagnosis of lung adenocarcinoma. *Anal Chem.* 2021;93(11):4984–92.
25. Han Y, Xia K, Su T. Exploration of the important role of Microfibrillar-Associated protein 4 gene in oral squamous cell carcinoma. *Med Sci Monit.* 2021;27:e931238.
26. Li J, Wang J, Liu Z, Guo H, Wei X, Wei Q et al. Tumor-suppressive role of microfibrillar associated protein 4 and its clinical significance as prognostic factor and diagnostic biomarker in hepatocellular carcinoma. (1998–4138 (Electronic)).
27. Zhao H, Sun Q, Li L, Zhou J, Zhang C, Hu T, et al. High expression levels of AGGF1 and MFAP4 predict primary Platinum-Based chemoresistance and are associated with adverse prognosis in patients with serous ovarian Cancer. *J Cancer.* 2019;10(2):397–407.
28. Zhao Z, Ma X, Sung D, Li M, Kosti A, Lin G, et al. microRNA-449a functions as a tumor suppressor in neuroblastoma through inducing cell differentiation and cell cycle arrest. *RNA Biol.* 2015;12(5):538–54.
29. Lv Y, Gao Y, Di W, Li Z, Shi Y, Hou T et al. MFAP4 is a novel prognostic biomarker in glioma correlating with immunotherapy resistance and ferroptosis. *Front Pharmacol.* 2025;16.
30. Nishimura Y, Takizawa R, Koike S, Kinoshita A, Satomura Y, Kawasaki S, et al. Association of decreased prefrontal hemodynamic response during a verbal fluency task with EGR3 gene polymorphism in patients with schizophrenia and in healthy individuals. *NeuroImage.* 2014;85(Pt 1):527–34.
31. Safford M, Collins S, Lutz MA, Allen A, Huang CT, Kowalski J, et al. Egr-2 and Egr-3 are negative regulators of T cell activation. *Nat Immunol.* 2005;6(5):472–80.
32. Li S, Miao T, Sebastian M, Bhullar P, Ghaffari E, Liu M, et al. The transcription factors Egr2 and Egr3 are essential for the control of inflammation and antigen-induced proliferation of B and T cells. *Immunity.* 2012;37(4):685–96.
33. Liu D, Evans I, Britton G, Zachary I. The zinc-finger transcription factor, early growth response 3, mediates VEGF-induced angiogenesis. *Oncogene.* 2008;27(21):2989–98.
34. Suzuki T, Inoue A, Fau - Miki Y, Miki Y, Fau - Moriya T, Moriya T, Fau - Akahira J-i, Akahira J Fau - Ishida T, Ishida T Fau - Hirakawa H, Early growth responsive gene 3 in human breast carcinoma: a regulator of estrogen-mediated invasion and a potent prognostic factor. (1351-0088 (Print)).
35. Xie Y, Han X, Yu J, Yuan M, Yan Y, Qin J et al. EGR3 and estrone are involved in the Tamoxifen resistance and progression of breast cancer. (1432– 1335 (Electronic)).
36. Hua Y, Wang H, Ye Z, Zheng D, Zhang X. An integrated pan-cancer analysis of identifying biomarkers about the EGR family genes in human carcinomas. *Comput Biol Med.* 2022;148:105889.
37. Knudsen AM, Eilertsen I, Kielland S, Pedersen MW, Sorensen MD, Dahlrot RH, et al. Expression and prognostic value of the transcription factors EGR1 and EGR3 in gliomas. *Sci Rep.* 2020;10(1):9285.
38. Liao F, Ji My Fau - Shen L, Shen L, Fau - Qiu S, Qiu S. Fau - Guo X-f, Guo Xf Fau - dong W-g, dong WG. Decreased EGR3 expression is related to poor prognosis in patients with gastric cancer. (1567–2387 (Electronic)).
39. Shin S-H, Kim I, Lee JE, Lee M, Park J-W. Loss of EGR3 is an independent risk factor for metastatic progression in prostate cancer. *Oncogene.* 2020;39(36):5839–54.
40. Symonds ALJ, Miao T, Busharat Z, Li S, Wang P. Egr2 and 3 maintain anti-tumour responses of exhausted tumour infiltrating CD8+ T cells. *Cancer Immunol Immunother.* 2023;72(5):1139–51.
41. Aghaei M, Khademi R, Bahreiny SS, Saki N. The need to Establish and recognize the field of clinical laboratory science (CLS) as an essential field in advancing clinical goals. *Health Sci Rep.* 2024;7(8):e70008.
42. Saki N, Haybar H, Aghaei M, Subject. Motivation can be suppressed, but scientific ability cannot and should not be ignored. *J Transl Med.* 2023;21(1):520.
43. Schussler MH, Skoudy A, Ramaekers F, Real FX. Intermediate filaments as differentiation markers of normal pancreas and pancreas cancer. *Am J Pathol.* 1992;140(3):559–68.
44. Shi JW, Liu W, Zhang TT, Wang SC, Lin XL, Li J, et al. The enforced expression of c-Myc in pig fibroblasts triggers mesenchymal-epithelial transition (MET) via F-actin reorganization and RhoA/Rock pathway inactivation. *Cell Cycle.* 2013;12(7):1119–27.

45. Zhou D, Duan Z, Li Z, Ge F, Wei R, Kong L. The significance of Glycolysis in tumor progression and its relationship with the tumor microenvironment. *Front Pharmacol*. 2022;13:1091779.
46. Metelli A, Wu BX, Fugle CW, Rachidi S, Sun S, Zhang Y et al. Surface expression of TGF β Docking receptor GARP promotes oncogenesis and immune tolerance in breast Cancer. (1538–7445 (Electronic)).
47. Yang L, Pang Y, Fau - Moses HL, Moses HL. TGF-beta and immune cells: an important regulatory axis in the tumor microenvironment and progression. (1471–4981 (Electronic)).
48. Kiryu S, Ito Z, Suka M, Bito T, Kan S, Uchiyama K, et al. Prognostic value of immune factors in the tumor microenvironment of patients with pancreatic ductal adenocarcinoma. *BMC Cancer*. 2021;21(1):1197.
49. Zhang QA-O, Sioud M. Tumor-Associated macrophage subsets: shaping polarization and targeting. LID– 10.3390/ijms24087493 [doi] LID– 7493. (1422–0067 (Electronic)).
50. Brummel K, Eerkens AL, de Bruyn M, Nijman HW. Tumour-infiltrating lymphocytes: from prognosis to treatment selection. *Br J Cancer*. 2023;128(3):451–8.
51. Karjalainen H, Sirnio P, Tuomisto A, Makinen MJ, Vayrynen JP. A prognostic score based on B cell and plasma cell densities compared to T cell densities in colorectal cancer. *Int J Colorectal Dis*. 2023;38(1):47.
52. Sakaguchi A, Horimoto Y, Onagi H, Ikarashi D, Nakayama T, Nakatsura T, et al. Plasma cell infiltration and treatment effect in breast cancer patients treated with neoadjuvant chemotherapy. *Breast Cancer Res*. 2021;23(1):99.
53. Gilbert AE, Karagiannis P, Fau - Dodev T, Dodev T, Fau - Koers A, Koers A, Fau - Lacy K, Lacy K. Fau - Josephs DH, Josephs Dh Fau - Takhar P. Monitoring the systemic human memory B cell compartment of melanoma patients for anti-tumor IgG antibodies. (1932–6203 (Electronic)).
54. Carmi Y, Spitzer MH, Linde IL, Burt BM, Prestwood TR, Perlman N et al. Allogeneic IgG combined with dendritic cell stimuli induce antitumour T-cell immunity. (1476–4687 (Electronic)).
55. Roumenina LA-O, Daugan MV, Petitprez FA-O, Sautès-Fridman CA-O, Fridman WA-O. Context-dependent roles of complement in cancer. (1474–768 (Electronic)).
56. Sivakumar S, Jainarayanan A, Arbe-Barnes E, Sharma PK, Leathlobhair MN, Amin S, et al. Distinct immune cell infiltration patterns in pancreatic ductal adenocarcinoma (PDAC) exhibit divergent immune cell selection and immunosuppressive mechanisms. *Nat Commun*. 2025;16(1):1397.
57. Zhang Y, Zou J, Chen R. An M0 macrophage-related prognostic model for hepatocellular carcinoma. *BMC Cancer*. 2022;22(1):791.
58. Gabrusiewicz K, Rodriguez B, Wei J, Hashimoto Y, Healy LM, Maiti SN et al. Glioblastoma-infiltrated innate immune cells resemble M0 macrophage phenotype. *JCI Insight*. 2016;1(2).
59. Zhang Q, Li H, Mao Y, Wang X, Zhang X, Yu X, et al. Apoptotic SKOV3 cells stimulate M0 macrophages to differentiate into M2 macrophages and promote the proliferation and migration of ovarian cancer cells by activating the ERK signaling pathway. *Int J Mol Med*. 2020;45(1):10–22.
60. Jairath NK, Farha MW, Jairath R, Harms PW, Tsoi LC, Tejasvi T. Prognostic value of intratumoral lymphocyte-to-monocyte ratio and M0 macrophage enrichment in tumor immune microenvironment of melanoma. *Melanoma Manag*. 2020;7(4):MMT51.
61. Tekin C, Aberson HL, Bijlsma MF, Spek CA. Early macrophage infiltrates impair pancreatic cancer cell growth by TNF-alpha secretion. *BMC Cancer*. 2020;20(1):1183.

Publisher's note

Springer Nature remains neutral with regard to jurisdictional claims in published maps and institutional affiliations.